

1 **The genome of the camphor tree and the genetic and climatic relevance of the**
2 **top-geoherbalism in this medicinal plant**

3
4 Rihong Jiang^{1,3,†}, Xinlian Chen^{2,4,†}, Xuezhu Liao², Dan Peng², Xiaoxu Han², Changsan
5 Zhu¹, Ping Wang³, David E. Hufnagel⁶, Cheng Li^{2,*}, Kaixiang Li^{1,*}, Li Wang^{2,5,*}

6
7 ¹Guangxi Engineering and Technology Research Center for Woody Spices, Guangxi
8 Key Laboratory for Cultivation and Utilization of Special Non-Timber Forest Crops,
9 Guangxi Forestry Research Institute, Nanning, China

10 ²Shenzhen Branch, Guangdong Laboratory for Lingnan Modern Agriculture, Genome
11 Analysis Laboratory of the Ministry of Agriculture, Agricultural Genomics Institute at
12 Shenzhen, Chinese Academy of Agricultural Sciences, Shenzhen, China

13 ³College of Environmental Sciences and Engineering, Central South University of
14 Forestry and Technology, Changsha, China

15 ⁴School of Pharmaceutical Sciences, Sun Yat-Sen University, Guangzhou, China

16 ⁵Kunpeng Institute of Modern Agriculture at Foshan, Foshan, China

17 ⁶Virus and Prion Research Unit, National Animal Disease Center, USDA-ARS, Ames,
18 USA

19 †These authors are contributed equally to this work.

20 *Correspondence (email wangli03@caas.cn (LW); email lkx202@126.com (KXL);
21 email licheng@caas.cn (CL))

22
23 **Abstract**

24 Camphor tree (*Cinnamomum camphora* (L.) J. Presl), a species in the magnoliid
25 family Lauraceae, is known for its rich volatile oils and is used as a medical
26 cardiotoxic and as a scent in many perfumed hygiene products. Here, we present a
27 high-quality chromosome-scale genome of *C. camphora* with a scaffold N50 of 64.34
28 Mb and an assembled genome size of 755.41 Mb. Phylogenetic inference revealed
29 that the magnoliids are a sister group to the clade of eudicots and monocots.
30 Comparative genomic analyses identified two rounds of ancient whole-genome
31 duplication (WGD). Tandem duplicated genes exhibited a higher evolutionary rate, a
32 more recent evolutionary history and a more clustered distribution on chromosomes,
33 contributing to the production of secondary metabolites, especially monoterpenes and
34 sesquiterpenes, which are the principal essential oil components. Three-dimensional
35 analyses of the volatile metabolites, gene expression and climate data of samples
36 with the same genotype grown in different locations showed that low temperature and
37 low precipitation during the cold season modulate the expression of genes in the
38 terpenoid biosynthesis pathways, especially *TPS* genes, which facilitates the
39 accumulation of volatile compounds. Our study lays a theoretical foundation for
40 policy-making regarding the agroforestry applications of camphor tree.

41
42 **Keywords:** *Cinnamomum camphora*, genome, top-geoherbalism, tandem duplication,
43 climatic factors

44

45 Introduction

46 Top-geoherbalism, also known as “Daodi” in China and “Provenance” or “Terroir” in
47 Europe, refers to traditional herbs grown in certain native ranges with better quality
48 and efficacy than those grown elsewhere, in which the relevant characteristics are
49 selected and shaped by thousands of years of the clinical application of traditional
50 medicine (Brinckmann, 2015). The concept of top-geoherbalism is documented in the
51 most ancient and classic Chinese Materia Medica (Divine Husbandman’s Classic of
52 Materia Medica; *Shen Nong Ben Cao Jing*) from approximately 221 B.C. to 220 A.D.
53 (Zhao et al., 2012), which reported that the origin and growing conditions of most
54 herbs were linked to their quality. Historical literature documented cases where the
55 misuse of traditional Chinese medicine (TCM) in prescriptions led to a reduction or
56 absence of therapeutic effects. For example, the application of dried tender shoots of
57 *Cinnamomum cassia* Presl (a component of *Guizhi soup* recorded in *Prescriptions for*
58 *Emergencies*) from non-top-geoherb regions led to a deficiency in the treatment of
59 fever, while the replacement of this TCM with materials from top-geoherb regions
60 results in proper fever treatment. Currently, TCM from top-geoherb regions accounts
61 for 80% of the market occupancy and economic profits of all TCMs (Huang, 2012),
62 and the significance of top-geoherbs has been revived by the increasing trend of the
63 protection of botanicals with “geographical indication” (GI) (Brinckmann, 2015). Thus,
64 a deep understanding of the pattern and mechanism of top-geoherbalism will strongly
65 guide producers and consumers of TCM and improve the standardization and
66 internalization of the TCM market, especially in the economic context of the Belt and
67 Road Initiative (Hinsley et al., 2020).

68 A substantial basis of the top-geoherbalism of TCMs is secondary metabolites that
69 play principal roles in the therapeutic effects of herbs. The content of secondary
70 metabolites is a continuous quantitative trait that is determined by three factors:
71 genotype, environment and the interaction between the genotype and environment. Li
72 et al. (2020) showed that cultivars of opium poppy with similar copy number variations
73 in benzyloisoquinoline alkaloid biosynthetic genes were likely to exhibit similar alkaloid
74 contents. To identify the ecological and climatic factors driving the development
75 top-geoherbs, the appropriate strategy is to grow herbs with the same genotype
76 (eliminating the effect of genetic variation) in different environmental settings and
77 study how environmental factors are correlated with secondary metabolites by altering
78 gene expression. However, most published studies confound the effects of genetic
79 variation and environmental factors. For example, Tan et al. (2015) identified
80 metabolite markers for distinguishing *Radix Angelica sinensis* from top-geoherb
81 regions and non-top-geoherb regions by analysing the volatile metabolites of
82 processed herbal medicine from drug stores in different regions. The roots of *Paeonia*
83 *veitchii* showed higher bioactivities when grown at lower average annual
84 temperatures and high elevations based on the analyses of environmental factors and
85 phytochemicals of different samples from seven populations (Yuan et al., 2020). Liu et
86 al. (2020) revealed a correlation between iridoid accumulation and increased
87 temperature by examining 441 individuals from 45 different origins. The confounding

88 factor of genetic variation led to the misinterpretation of how environmental factors
89 alone affect secondary metabolites. In addition, top-geoherb TCMs have been
90 annotated with their cultural properties, including their cultivation, harvesting and
91 postharvest processing (Huang, 2012), which is outside of the scope of the current
92 study.

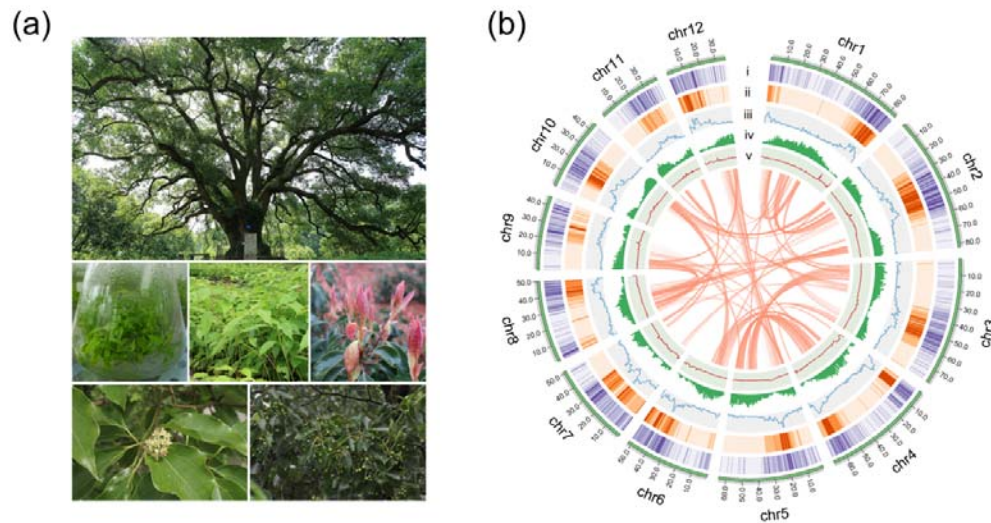
93 *Cinnamomum camphora* (L.) J. Presl (Figure 1a), also known as camphor tree is
94 native to China, India, Mongolia and Japan (Chen et al., 2017; Yoshida et al., 1969)
95 and was later introduced to Europe and the southern United States (Bottoni et al.,
96 2021; Hamidpour et al., 2012; Ravindran et al., 2004). Camphor trees are divided into
97 five chemotypes according to their dominant volatile oil components as linalool,
98 camphor, eucalyptol, borneol and isonerolidol types (Luo et al., 2021). Their leaves
99 are especially rich in volatile oil components, including monoterpenes, sesquiterpenes
100 and diterpenes (Hou et al., 2020; Tian et al., 2021). Camphor tree has high medicinal,
101 ornamental, ecological and economic value (Chen, 2020; Liu et al., 2019; Zhang et al.,
102 2020). As a TCM, *C. camphora* can be used to treat rheumatism and arthralgia, sores
103 and swelling, skin itching, poisonous insect bites, etc. Among the many chemical
104 components of the species, camphor is used as a cardiogenic, deodorant and
105 stabilizer in medicine, daily-use chemical production and industry, and linalool is most
106 frequently used as a scent in 60% to 80% of perfumed hygiene products and cleaning
107 agents (Consultation, 2021; Eggersdorfer, 2000; Letizia et al., 2003).

108 *C. camphora* belongs to Lauraceae within the magnoliid group comprising four
109 orders (Laurales, Magnoliales, Canellales and Piperales). Magnoliids are the third
110 largest group of angiosperms, including approximately 9,000-10,000 species
111 (Massoni et al., 2015; Palmer et al., 2004). From an evolutionary point of view, the
112 mysterious phylogenetic position of magnoliids within angiosperms has been debated
113 for decades. Recently, the debate on the phylogenetic position of magnoliids has
114 focused on three main topologies (Endress and Doyle, 2009; Moore et al., 2007; Qiu
115 et al., 2010; Zeng et al., 2014) positioning magnoliids as (a) a sister group to eudicots
116 (Chaw et al., 2019; Lv et al., 2020; Shang et al., 2020); (b) a sister group to monocots
117 (Qin et al., 2021); or (c) a sister group to the clade of monocots and eudicots (Chen et
118 al., 2019; Chen et al., 2020; Chen et al., 2020; Hu et al., 2019; Rendón-Anaya et al.,
119 2019). Furthermore, the different whole-genome duplication (WGD) events that have
120 occurred in specific lineages of magnoliids and the divergences time between
121 different magnoliid plants remain unclear (Chaw et al., 2019; Chen et al., 2019; Chen
122 et al., 2020; Chen et al., 2020; Hu et al., 2019; Lv et al., 2020; Qin et al., 2021;
123 Rendón-Anaya et al., 2019; Shang et al., 2020).

124 Despite the economic and evolutionary value of *C. camphora*, the lack of a
125 high-quality genome for the species has greatly restricted the progress of genetic
126 research and the identification of the biosynthetic genes underlying the production of
127 essential volatile compounds with medicinal effects (Chaw et al., 2019; Chen et al.,
128 2019; Chen et al., 2020; Chen et al., 2020; Hu et al., 2019; Lv et al., 2020;
129 Rendón-Anaya et al., 2019; Shang et al., 2020). In our study, we *de novo* assembled
130 the chromosome-scale genome of *C. camphora*, explored the genomic characteristics
131 of *C. camphora* and investigated the genetic and climatic factors underlying the

132 top-geothermalism of this well-known TCM.

133



134

135 **Figure 1** The camphor tree and landscape of its genome. (a) Images of a camphor tree and its multiple
136 tissues. (i) An ancient camphor tree, (ii) tissue-cultured seedlings, (iii) seedlings, (iv) young leaves, (v)
137 flowers and (vi) fruits. (b) Circos plot of the *C. camphora* genome assembly. Circles from outside to inside:
138 (i) chromosomes, (ii) *Gypsy* LTR density, (iii) *Copia* LTR density, (iii) total LTR density, (iv) gene density
139 and (v) GC content. These density metrics were calculated with 1 Mb nonoverlapped sliding windows.

140

The syntenic genomic blocks (>300 kb) are illustrated with orange lines.

141

142 Results

143 *C. camphora* genome assembly and annotation

144 A haplotype-resolved genome assembly was obtained by using Hifiasm (Cheng et al.,
145 2021) integrating HiFi long reads (24.95 Gb; ~32.83X based on a previous flow
146 cytometry-based estimated genome size of 760 Mb (Wu, 2014)) and Hi-C short reads
147 (63.78 Gb; ~83.92X) with the default parameters. The two contig-level haplotype
148 genomes showed total sizes of 768.97 Mb and 752.05 Mb, respectively, after
149 removing redundant sequences with Purge_haplotigs (Roach et al., 2018). Compared
150 with the earlier published *C. kanehirae* genome (Chaw et al., 2019), the contig N50
151 was 2.01 Mb for haplotype A and 2.25 Mb for haplotype B; these values are ~2.2- and
152 ~2.5-fold higher, respectively, than the values of the previously published *C.*
153 *kanehirae* genome (Chaw et al., 2019), respectively (Table 1). Benchmarking
154 Universal Single-Copy Orthologue (BUSCO) analyses showed that the contig sets of
155 haplotype A and haplotype B contained 94.1% and 96.0% complete sets of the core
156 orthologous genes of viridiplantae, respectively (Table S2). Subsequently, the two
157 nonredundant contig sets were anchored to 12 chromosomes based on Hi-C contacts
158 (Figure S1). Overall, the assembled genome size was consistent with previous
159 reports (Table 1; Table S3). As the chromosome-level haplotype A genome was much
160 closer to the estimated genome size than the haplotype B genome, it was used for
161 subsequent analyses.

162 The final assembled *C. camphora* genome consisted of 12 chromosomes, 1,025
163 scaffolds and 1,686 contigs, with a scaffold N50 of 64.34 Mb (Table 1; Figure 1b). The
164 number of assembled chromosomes was consistent with previous cytological
165 observations (<http://ccdb.tau.ac.il>). The length of the chromosomes ranged from
166 84.54 Mb (Chr1) to 36.36 Mb (Chr12) (Table S5). The high fidelity of the assembly
167 was corroborated by multiple lines of evidence. First, the mapping rates of RNA-Seq
168 paired-end reads against the assembled genome were high (93%-95%). Second, the
169 high completeness of this assembly was supported by a 96.2% BUSCO value (Table
170 1; Table S4), suggesting high completeness at the gene level, which was much better
171 than the completeness of the *C. kanehirae* genome assembled via PacBio CLR
172 sequencing. Third, the long terminal repeat (LTR) assembly index (LAI) score (Ou et
173 al., 2018) was 13.82, indicating the “reference” level of the genome and reflecting
174 completeness at the transposable element (TE) level.

175 By combining *ab initio* prediction, orthologous protein and transcriptomic data, we
176 annotated 24,883 protein-coding genes using the MAKER pipeline (Cantarel et al.,
177 2008) (Table 1). The average lengths of the gene regions, coding sequences (CDSs),
178 exon sequences, and intron sequences were 9,295.00, 1,189.59, 309.29, and
179 1,548.48 bp, respectively (Table 1). Among the predicted protein-coding genes,
180 97.06% could be annotated in at least one of the following protein-related databases:
181 NCBI nonredundant protein (NR) (97.04%), Swiss-Prot (80.87%), Pfam (72.12%), GO
182 (46.59%) or KEGG (45.08%) (Table 1).

183 A total of 361.37 Mb of TEs were identified (Table S6). Long-terminal repeat
184 retrotransposons (LTR-RTs) were the most abundant type of repetitive sequence,
185 accounting for 46.86% of the whole genome, similar to the proportion of LTRs found in
186 *C. kanehirae* (Table 1). A total of 3,731 intact LTR-RTs were identified, and the
187 frequency distribution of insertion times showed a burst of LTR-RTs 1-2 million years
188 ago (Mya) (Figure S2), consistent with previous reports in magnoliids. Gypsy
189 elements were the largest LTR-RT superfamily in *C. camphora*, constituting 15.42% of
190 the genome. The second largest superfamily was Copia, accounting for 7.69% of the
191 genome. Other unclassified LTR-RTs encompassed 4.83% of the genome. Among
192 DNA retrotransposons, terminal inverted repeat sequences (TIRs) and non-TIRs
193 comprised 14.05% and 5.87% of the genome, respectively.

194

Table 1 The statistics for genome assemblies of *Cinnamomum*

	<i>C. camphora</i>	<i>C. kanehirae</i>
Gene assembly		
Genome size (Mb)	755.41	730.43
Scaffold number (n)	1,037	2,153
Scaffold N50 (Mb)	64.34	50.35
Scaffold L51 (n)	5	6
Chromosome-scale scaffolds (Mb)	697.81 (92.38%)	672.85 (92.12%)
Contig number (n)	1,686	-
Contig N50 (Mb)	2.01	0.90
Contig L51 (n)	108	-
GC content of the genome (%)	39.49	38.22
Complete BUSCOs (%)	96.20	88.50
TE annotation		
TE content (%)	47.86	47.87
LTR content (%)	27.94	25.53
Copia content (%)	7.69	-
Gypsy content (%)	15.42	-
LAI	13.82	-
Gene annotation		
Number of predicted genes (n)	24,883	27,899
Average gene length (bp)	9,295.00	7,591.84
Average CDS length (bp)	1,189.59	1,310.51
Average exon length (bp)	309.29	241.55
Average exon number per transcript (n)	4.80	5.40
Average intron length (Mb)	1,548.48	1,425.80
Average intron number per transcript (n)	4.40	4.06
Gene function annotation		
Nr	24,147 (97.04%)	-
Swissprot	20,122 (80.87%)	-
Pfam	17,945 (72.12%)	-
GO	11,593 (46.59%)	-
KEGG	11,218 (45.08%)	-
Total	24,152 (97.06%)	-

The assembly for *C. camphora* was compared with *C. kanehirae*. Dash (-) indicates data were not shown in the original research.

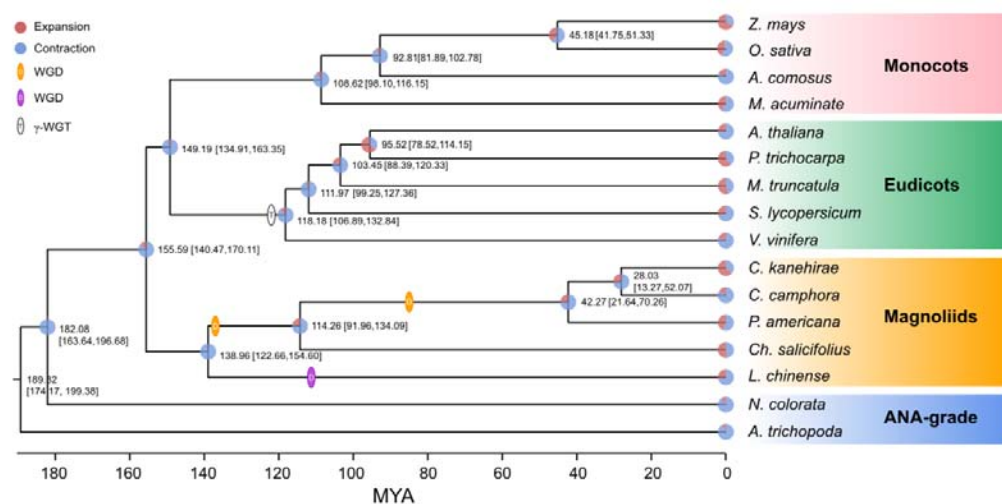
195

196

197 **Phylogenetic and WGD analyses**

198 The concatenate phylogenetic tree constructed with 172 single-copy orthologous
 199 genes among 16 species showed that *C. camphora* was clustered with two other
 200 Lauraceae species and that the formed clade was then clustered with other
 201 magnoliids (Figure 2; Figure S3a). More importantly, the magnoliids were sister to the
 202 combined clade of eudicots and monocots rather than to either monocots or eudicots.
 203 In addition, the coalescence-based phylogenetic tree showed the same topology for

204 magnoliids as the concatenation tree (Figure S3b). This phylogenetic topology is
 205 consistent with some previous studies (Chen et al., 2019; Chen et al., 2020; Chen et
 206 al., 2020; Hu et al., 2019; Rendón-Anaya et al., 2019) but contrasts with other reports
 207 (Chaw et al., 2019; Lv et al., 2020; Qin et al., 2021; Shang et al., 2020). The
 208 divergence time between magnoliids and the clade of monocots and eudicots was
 209 inferred to be 147.47-170.11 Mya (Figure 2) in MCMCTree with fossil calibration
 210 (Yang et al., 2007), coinciding with the estimates in other studies (Chen et al., 2019;
 211 Chen et al., 2020; Chen et al., 2020; Hu et al., 2019; Rendón-Anaya et al., 2019). In
 212 the clade of magnoliids, the divergence time between Laurales and Magnoliales was
 213 approximately 138.96 Mya, after which the divergence of Lauraceae and
 214 Calycanthaceae occurred approximately 114.26 Mya, and finally, *C. camphora*
 215 diverged from the most recent common ancestor of *C. camphora* and *C. kanehirae*
 216 approximately 28.03 Mya.
 217



218
 219 **Figure 2** Phylogenetic analyses. The phylogenetic tree was constructed based on 172 single-copy
 220 orthologous genes of 16 species using two ANA-grade species as outgroups; node age and 95%
 221 confidence intervals are labeled. Pie charts show the proportions of gene families that underwent
 222 expansion or contraction. Predicted whole-genome duplication (WGD) events were only indicated for
 223 Laurales and Magnoliales.
 224

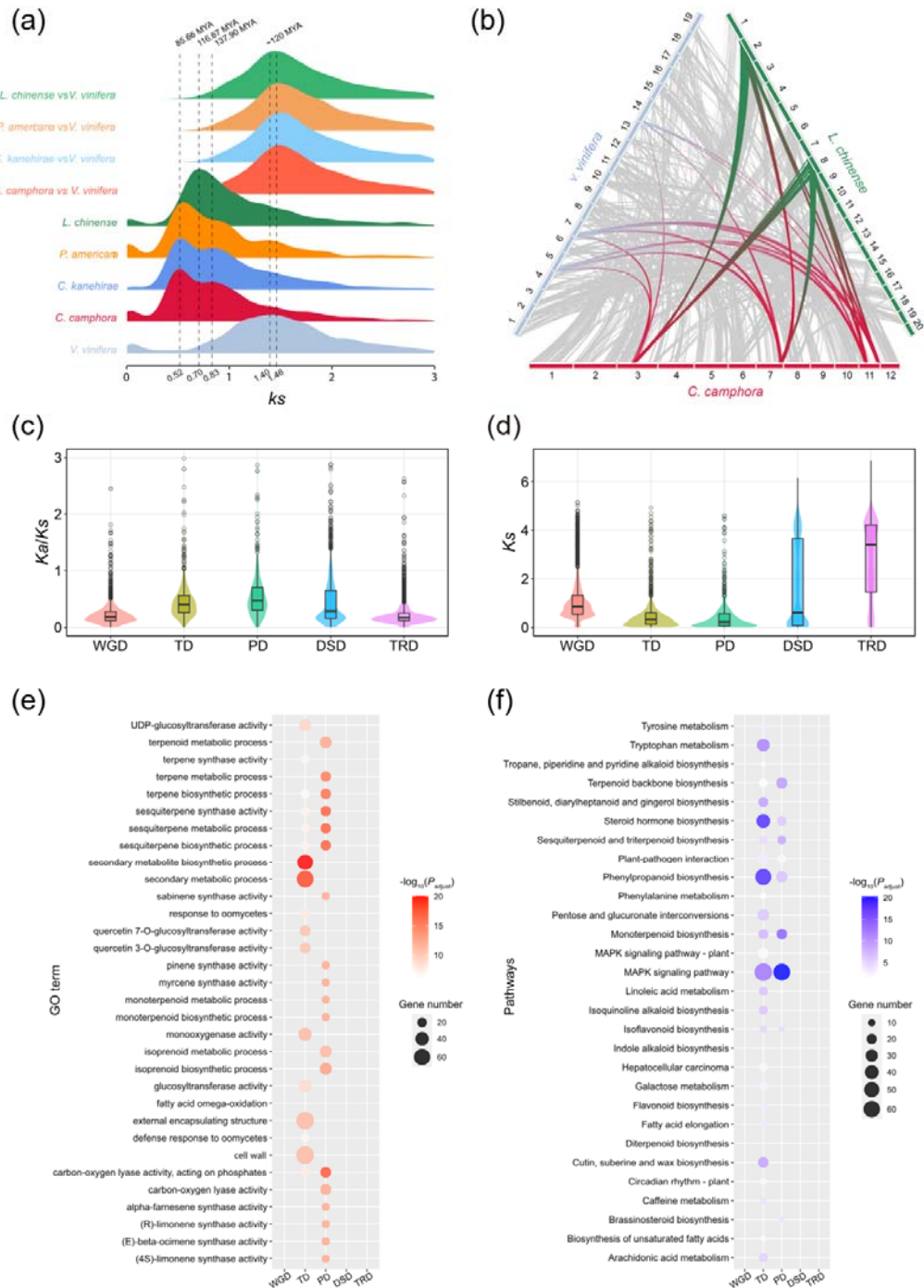
225 The intragenomic collinearity and syntenic depth ratio of *C. camphora* showed clear
 226 syntenic evidence of ancient WGD events (Figure 1b; Figure S4). Only the paralogous
 227 gene set derived from duplicates produced by WGD was used for the analyses of
 228 synonymous substitutions per site (*K_s*) (see “Methods” section). Two ancient WGD
 229 events shared within the Laurales lineage (*C. camphora*, *C. kanehirae* and *Persea*
 230 *americana*) occurred approximately 85.66 Mya and 137.90 Mya, represented by two
 231 signature peaks with *K_s* values of approximately 0.52 and 0.83 (Figure 3a). The
 232 recent *K_s* peak (85.66 Mya) occurred much earlier than the divergence time (42.27
 233 Mya) between *P. americana* and the common ancestor of *Cinnamomum*, indicating
 234 that this round of WGD was shared between *Cinnamomum* and *Persea* (Figure 2;

235 Figure 3a). Additionally, the *Ks* peak (137.90 Mya) occurred earlier than the
236 divergence (114.26 Mya) between Lauraceae species and *Chimonanthus salicifolius*,
237 implying that this round of WGD was shared between Lauraceae and Calycanthaceae
238 (Figure 2; Figure 3a). We also detected a WGD event in *Liriodendron chinense* that
239 occurred approximately 116.67 Mya, corresponding to a *Ks* peak of 0.70 (Figure 3a),
240 which is consistent with a previous study (Chen et al., 2019).

241 To confirm that *C. camphora* underwent two rounds of ancient WGD, we performed
242 intergenomic synteny analyses between the genomes of *C. camphora* and *L.*
243 *chinense* together with *Vitis vinifera*. A “4:2” syntenic relationship was detected
244 between *C. camphora* and *L. chinense* (Figure S5a). Given the hexaploidy event
245 (γ -WGT) shared among core eudicots, including *V. vinifera* (French-Italian Public
246 Consortium for Grapevine Genome Characterization, 2007), an overall “4:3” syntenic
247 relationship was observed between *C. camphora* and *V. vinifera* (Figure S5b).
248 Furthermore, we discovered a “2:3” syntenic relationship between *L. chinense* and *V.*
249 *vinifera* (Figure S5c). Thus, the syntenic relationships among the *L. chinense*:*V.*
250 *vinifera*:*C. camphora* genomes showed a 2:3:4 ratio (Figure 3b). Our results echoed
251 previous studies (Chaw et al., 2019; Chen et al., 2019), indicating two rounds of
252 ancient WGD in Lauraceae.

253 To determine the functional roles of the genes retained after WGD events, GO and
254 KEGG enrichment analyses were performed. The results showed that the genes
255 retained after WGD were enriched in basic physiological activities, processes and
256 pathways, such as structural constituents of ribosomes, NADPH dehydrogenase
257 activity, photosynthesis and plant hormone signal transduction, suggesting that two
258 rounds of WGD events enhanced the adaptability of *C. camphora* to changing
259 environments by improving basic physiological activities and primary metabolism
260 (Figure S6; Figure S7; Table S7; Table S12).

261



262

263

264

265

266

267

268

269

Figure 3 Gene duplication and evolution. (a) Ks distribution of paralogues in magnoliid species (*C. camphora*, *C. kanehirae*, *P. americana* and *L. chinense*) and orthologues between these magnoliids and *V. vinifera*. (b) Synteny blocks among *C. camphora*, *L. chinense* and *V. vinifera*. (c) Ka/Ks ratio distributions of gene pairs derived from different types of duplication. WGD, whole-genome duplication; TD, tandem duplication; PD, proximal duplication; TRD, transposed duplication; DSD, dispersed duplication. (d) Ks ratio distributions of gene pairs derived from different types of duplication. (e) GO enrichment analyses of genes from different types of duplication. The enriched GO terms with adjusted P

270 values < 0.01 are presented. The colours of the bubbles indicate the statistical significance of the
271 enriched GO terms. The sizes of the bubbles indicate the number of genes associated with one GO term.
272 (f) KEGG enrichment analyses of genes resulting from different types of duplication. Enriched KEGG
273 pathways with adjusted *P* values < 0.01 are presented. The colours of the bubbles represent the
274 statistical significance of enriched KEGG pathways. The sizes of the bubbles indicate the number of
275 genes associated with one KEGG pathway.

276

277 **Tandem and proximal duplications contribute to terpene synthesis in *C.*** 278 ***camphora***

279 A total of 18,938 duplicated genes were identified, including 7,043 WGD genes
280 (37.19%), 1,597 tandem duplication (TD) genes (8.43%), 1,079 proximal duplication
281 (PD) genes (5.70%), 5,127 dispersed duplication (DSD) genes (27.07%) and 3,779
282 transposed duplication (TRD) genes (19.95%) (Figure S8). The *K_s* and *K_a/K_s* values
283 among different types of duplicated genes were calculated (Figure 3c; Figure 3d). The
284 *K_s* values of TD and PD genes were much smaller than those of other types of
285 duplications (Figure 3d), suggesting that TD and PD genes were formed recently.
286 Additionally, the higher *K_a/K_s* ratios of TD and PD genes (Figure 3c) implies that they
287 were subject to more rapid sequence divergence.

288 We also performed GO and KEGG enrichment analyses of the gene sets
289 associated with the five duplication types (Figure S6; Figure S7; Table S7-S16). The
290 GO results showed that the biological process (BP) and molecular function (MF)
291 categories of secondary metabolite, monoterpene, sesquiterpene and terpene
292 biosynthesis and metabolism were significantly enriched in the TD and PD gene sets,
293 but no enrichment of these GO terms was found in the WGD, DSD and TRD gene
294 sets (Figure 3e). Regarding the KEGG results, the TD and PD gene sets were
295 significantly enriched in the terpenoid backbone, monoterpenoid, sesquiterpenoid and
296 phenylpropanoid biosynthesis pathways. These secondary metabolite biosynthesis
297 pathways were not enriched in the other three duplication gene sets (Figure 3f). In
298 addition, KEGG pathways related to responses to environmental stimuli, such as the
299 MAPK signalling pathway, steroid hormone biosynthesis and plant-pathogen
300 interaction, were also significantly enriched in the TD and PD gene sets. All of these
301 results indicated that the rapidly evolving TD and PD genes played essential roles in
302 the synthesis of secondary metabolites, especially monoterpenes and sesquiterpenes,
303 and the response to environmental stimuli in *C. camphora*.

304

305 **Metabolic reflection of top-geoherbalism**

306 To evaluate how environmental factors affect metabolite accumulation, we grew
307 tissue-cultured seedlings from a single mother plant in four major production locations,
308 including Qinzhou, Nanning, Baise and Liuzhou, beginning in May 2018. Mature
309 leaves were harvested from the four locations in November 2020 for RNA-Seq and
310 metabolite assessment. Thus, we were able to compare the effects of environmental
311 conditions on metabolite accumulation based on the fixed genotype.

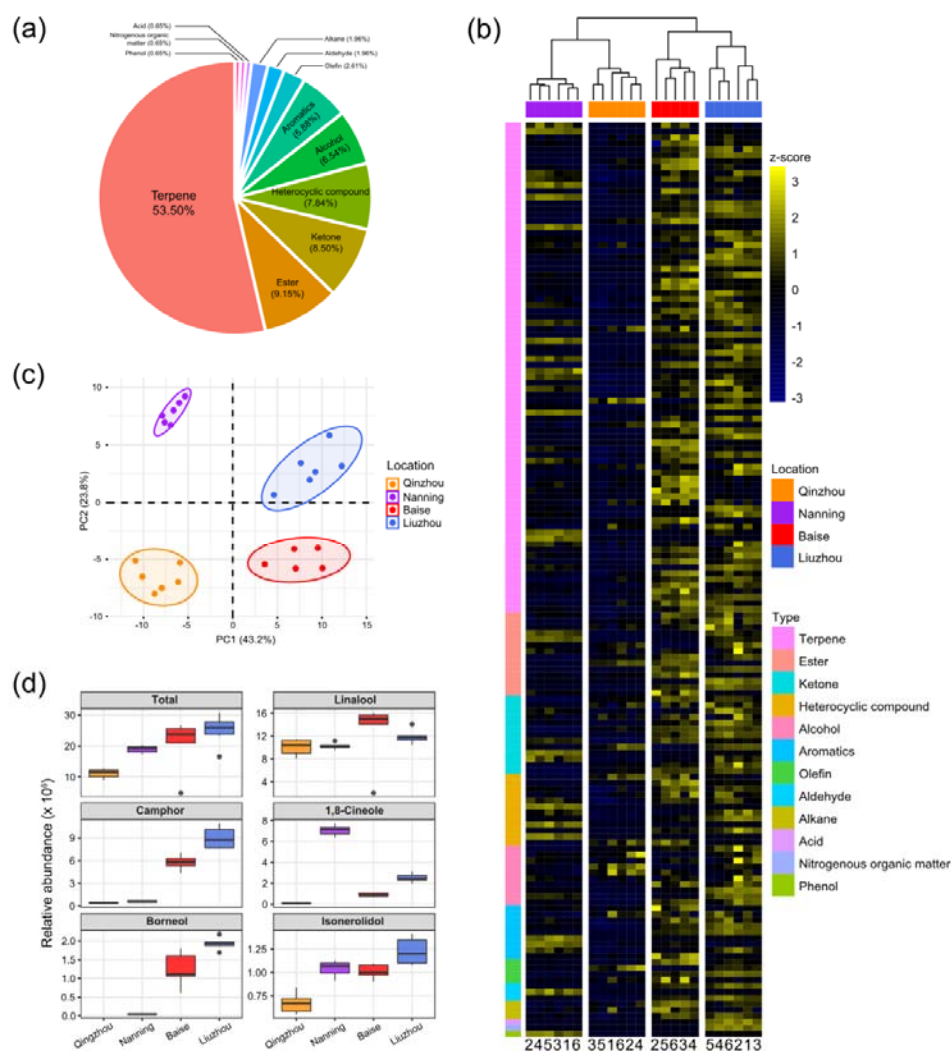
312 Volatile metabolites are a substantial basis of the top-geoherbalism of camphor tree.
313 Based on targeted gas chromatography-mass spectrometry (GC-MS) analyses, we

314 identified 153 nonredundant volatile metabolites (Supplemental Table 17). The 153
315 volatile metabolites included 82 terpenes (53.60%), 14 esters (9.15%), 13 ketones
316 (8.50%), 12 heterocyclic compounds (7.84%), 10 alcohols (6.54%), 9 aromatics
317 (5.88%) and 13 additional metabolites (8.49%) that did not belong to these six main
318 types (Figure 4a). For quality control, we performed hierarchical clustering and
319 principal component analyses (PCA) of metabolic abundances in these 24 samples
320 (Figure S9). The first replicate in Baise (“Baise_1”) was identified as an outlier and
321 was removed from further analyses.

322 The volatile metabolites of the samples from the four locations exhibited distinct
323 clustering in the PCA plot (Figure 4c). Notably, the metabolites of samples from Baise
324 and Liuzhou were clearly separated from those of Qinzhou and Nanning according to
325 principal component 1 (PC1), which accounted for 43.2% of the total variance. The
326 heatmap based on the relative abundances of volatile metabolites showed that
327 samples from Baise and Liuzhou exhibited higher abundances than those from
328 Qinzhou and Nanning, especially with regard to terpenes (Figure 4b; Figure S10).

329 Linalool, borneol, camphor, 1,8-cineole and isonerolidol are the five main
330 phytochemicals determining the medicinal value and top-geoherbalism of *C.*
331 *camphora*. A detailed comparison of the five volatile terpenoids implied that samples
332 from Liuzhou showed the highest total abundance, followed by the samples from
333 Baise, while the abundance was lowest in Qinzhou (Figure 4d). The abundance
334 profiling of camphor and borneol in the four locations echoed the trends of the total
335 abundance of the five volatile terpenoids. The abundance of linalool and isonerolidol
336 peaked in Baise and Liuzhou, respectively, while that of 1,8-cineole peaked in
337 Nanning. Taken together, these results suggested that Baise and Liuzhou are
338 top-geoherb regions of the camphor tree in Guangxi Province.

339



340
 341 **Figure 4** Abundance patterns of volatile metabolites in *C. camphora* planted in different locations. (a) Pie
 342 charts show the proportions of different types of metabolites identified in the current study. (b)
 343 Hierarchical clustering heatmap of metabolic abundance profiles in the four planting locations, including
 344 Qinzhou, Nanning, Baise and Liuzhou, indicated on the x axis. Metabolic abundance was averaged and
 345 z-score transformed. The rows are clustered by the types of metabolites. (c) Principal component
 346 analyses (PCA) of metabolites of *C. camphora* planted in the four locations. The circles represent the
 347 95% confidence intervals. (d) The relative abundances of linalool, borneol, camphor, 1,8-cineole and
 348 isonerolidol in the four planting locations.

349

350 Modulation of gene expression related to top-geoherbalism

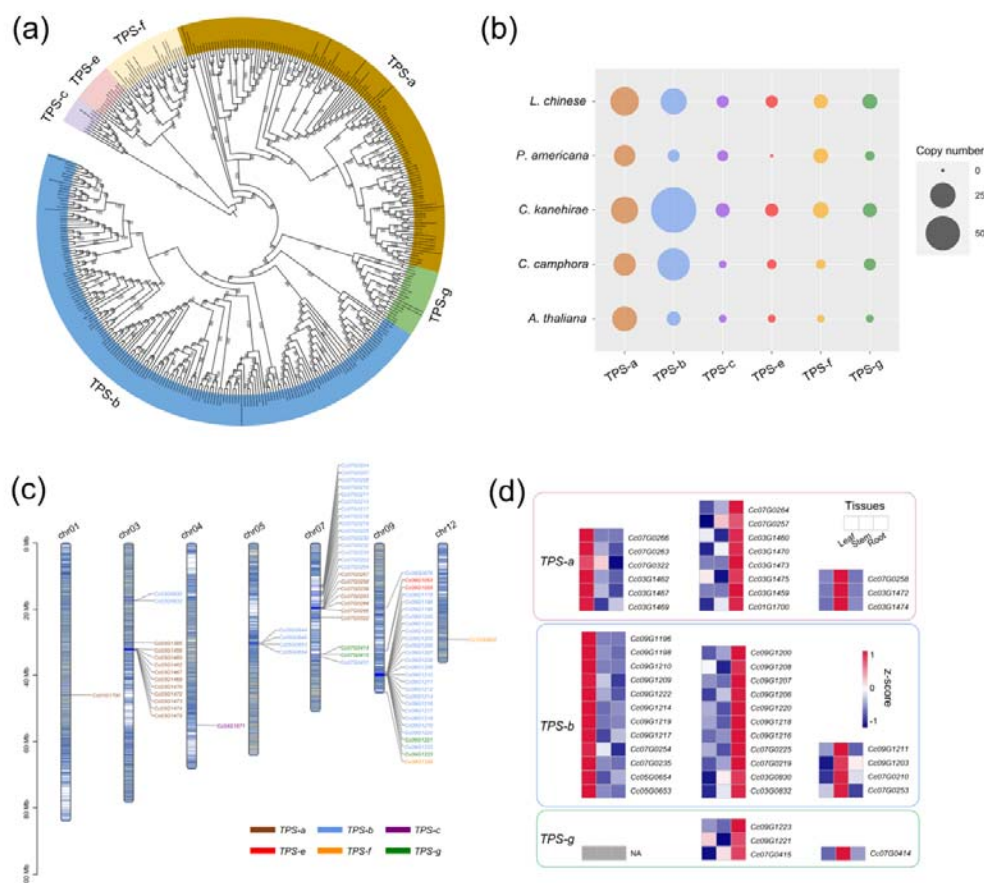
351 TPSs are the rate-limiting enzymes in the production of terpenoids (Chen et al., 2011;
 352 Tholl, 2015), including monoterpenes, sesquiterpenes and diterpenoids (see
 353 “Methods” section). The identified *TPS* genes of *C. camphora*, *C. kanehirae*, *P.*
 354 *americana*, *L. chinense* and *Arabidopsis thaliana* were clustered into six clades in the
 355 phylogenetic tree, corresponding to the *TPS-a*, *TPS-b*, *TPS-c*, *TPS-e*, *TPS-f* and
 356 *TPS-g* subfamilies (Chen et al., 2011), among which *TPS-b* and *TPS-g* encode the

357 enzymes catalysing the production of 10-carbon monoterpenoids from geranyl
358 diphosphate (GPP), and *TPS-a* genes are responsible for catalysing the production of
359 15-carbon sesquiterpenoids from farnesyl diphosphate (FPP) (Figure 5a,b). The copy
360 number variation of the *TPS* genes showed that *TPS-b* was greatly expanded in *C.*
361 *kanehirae* and *C. camphora* (Figure 5a,b), which resulted in the high abundance of
362 monoterpenoids in *Cinnamomum* (Chen et al., 2020; Chen et al., 2020). Specifically,
363 44 *TPS-b* genes were identified in *C. camphora*, accounting for 61% of all its *TPS*
364 genes, consistent with the percentage observed in *C. kanehirae* (63%) and much
365 higher than those in *L. chinense* (33%), *A. thaliana* (18%) and *P. americana* (12%).
366 We also observed more copies of the *TPS-g* subfamily in *C. camphora* than in *A.*
367 *thaliana* and *P. americana*. However, no expansion of *TPS-a* genes was detected in
368 *Cinnamomum*.

369 Next, we examined how the *TPS* genes were distributed across the genome.
370 Chromosome 9 and chromosome 7 harboured the most *TPS* genes (27 and 25,
371 respectively), followed by chromosome 3 (13 *TPS* genes) (Figure 5c; Table S18).
372 Interestingly, genes from the seven subfamilies were observed as tandem duplicates.
373 Two large *TPS-b* gene clusters were identified on chromosome 9 (21 genes; ca.
374 38.78-40.12 Mb) and chromosome 7 (10 genes; ca. 12.70-16.03 Mb), respectively. In
375 addition, two large *TPS-a* gene clusters were detected on chromosome 3 (10 genes;
376 ca. 31.90-32.52 Mb) and chromosome 7 (6 genes; ca. 19.49-19.90 Mb), respectively.
377 The remaining smaller *TPS* gene clusters were scattered throughout the genome of *C.*
378 *camphora*.

379 Notably, the *TPS* genes exhibited a strong tissue-specific expression pattern
380 (Figure 5d; Table S19), especially *TPS-a*, *TPS-b* and *TPS-g*. We downloaded
381 previously published RNA-Seq data
382 (<https://www.ncbi.nlm.nih.gov/bioproject/PRJNA747104>) from three tissues (leaf,
383 stem and root) of *C. camphora* to determine the gene expression profile of *TPS* genes.
384 As leaves are the major tissue used in medicine, we focused on the *TPS* genes with
385 high expression levels in leaves. Six *TPS-a* genes and twelve *TPS-b* genes showed
386 higher expression in leaves than in stems and roots. All of these results indicated that
387 the expansion of the *TPS-b* subfamily and the tandem duplication of *TPS-b* genes
388 probably contribute to monoterpenoid biosynthesis in *C. camphora*.

389



390

391

Figure 5 Genes involved in the biosynthesis of volatile terpenoids. (a) Phylogenetic analyses of *TPS*

genes in *C. camphora*. The phylogenetic tree was constructed based on *TPS* gene sequences from four

magnoliid genomes (*C. camphora*, *C. kanehirae*, *P. americana* and *L. chinense*) and *A. thaliana*. (b)

Copy numbers of *TPS* genes in the genomes of four magnoliids and *A. thaliana*. (c) Distribution of the

TPS genes on seven chromosomes of *C. camphora*. (d) Tissue-specific expressions of *TPS-a*, *TPS-b*

and *TPS-g* subfamilies.

396

397

398

The biosynthetic pathways of terpenoids are derived from isopentenyl diphosphate

(IPP) and dimethylallyl diphosphate (DMAPP) produced via the methylerythritol

phosphate (MEP) and mevalonate (MVA) pathways, respectively (Li et al., 2019; Zhou

and Pichersky, 2020). Comparative transcriptome analyses of samples from the four

locations were performed to examine the expression patterns of genes involved in the

MEP and MVA pathways. We combined four differentially expressed gene (DEG) sets

identified in Liuzhou vs. Qinzhou, Liuzhou vs. Nanning, Baise vs. Qinzhou and Baise

vs. Nanning (Figure S11). We detected 22 and 23 DEGs in the MEP and MVA

pathways, respectively (Figure 6; Table S20). Generally, the DEGs involved in all the

steps of the MEP and MVA pathways showed higher expression in Baise and Liuzhou

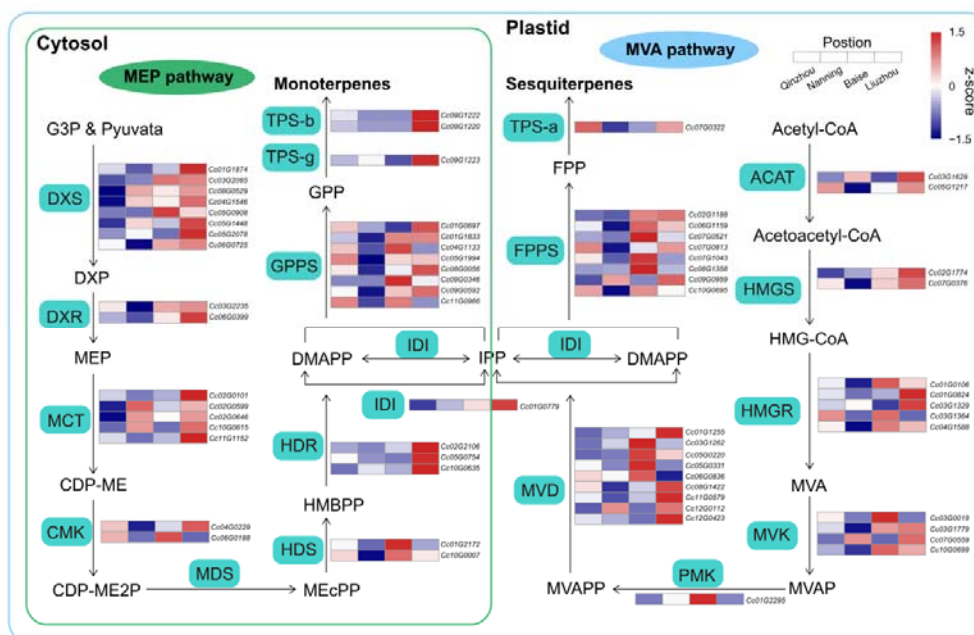
than in Qinzhou and Nanning, except for the

2-C-methyl-D-erythritol-2,4-cyclodiphosphate synthase (MDS) gene, which was

absent in the combined DEG set. The same expression pattern was observed for the

410

411 genes related to downstream steps, including *isopentenyl diphosphate isomerase*
 412 (*IDI*), *geranyl diphosphate synthetase* (*GPPS*), *farnesyl diphosphate synthetase*
 413 (*FPPS*), *TPS-a*, *TPS-b* and *TPS-g*. The modulation of gene expression in the
 414 terpenoid biosynthesis pathway echoed the higher accumulation of monoterpenoids
 415 and sesquiterpenoids observed in Baise and Liuzhou than in Qinzhou and Nanning.
 416



417
 418 **Figure 6** Biosynthetic pathways of monoterpenoids and sesquiterpenoids. Relative expression profiling
 419 of genes involved in volatile terpenoid biosynthesis among the four planting locations (Qinzhou, Nanning,
 420 Baise and Liuzhou). Gene expression was extracted from the combined differentially expressed gene
 421 (DEG) set (Liuzhou vs. Qinzhou, Liuzhou vs. Nanning, Baise vs. Qinzhou and Baise vs. Nanning). MEP,
 422 mevalonate pathway; MEP, methylerythritol phosphate pathway; ACAT, acyl-coenzyme A-cholesterol
 423 acyl-transferase; HMGS, hydroxymethylglutaryl coenzyme A synthase; HMGR, hydroxymethylglutaryl
 424 coenzyme A reductase; MVK, mevalonate kinase; PMK, phospho-mevalonate kinase; MVD, mevalonate
 425 diphosphate decarboxylase; DXS, 1-deoxy-D-xylulose 5-phosphate synthase; DXR, 1-deoxy-D-xylulose
 426 5-phosphate reductoisomerase; MCT, 2-C-methyl-D-erythritol-4-phosphate cytidyltransferase; CMK,
 427 4-(cytidine-5-diphospho)-2-C-methyl-D-erythritol kinase; MDS,
 428 2-C-methyl-D-erythritol-2,4-cyclodiphosphate synthase; HDS,
 429 (E)-4-hydroxy-3-methyl-but-2-enyl-pyrophosphate synthase; HDR,
 430 (E)-4-hydroxy-3-methyl-but-2-enyl-pyrophosphate reductase.

432 Climatic factors underlying the top-geoherbalism of *C. camphora*

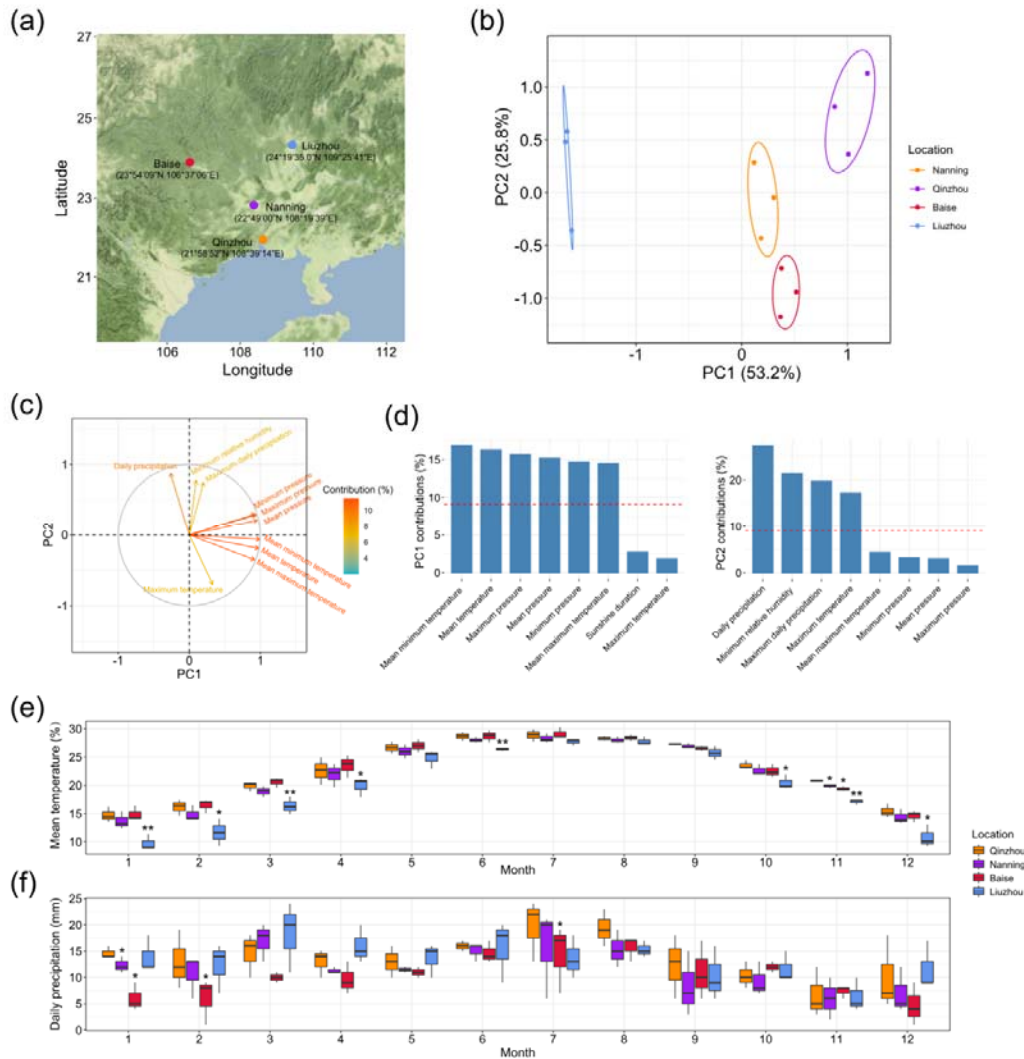
433 To determine what climatic factors caused the differences in volatile metabolites
 434 among the *C. camphora* plants of the same genotype grown in different locations
 435 (Figure 7a), we downloaded the climate data of Qinzhou, Nanning, Baise and Liuzhou
 436 from three years (2018-2020) from the National Meteorological Information Centre
 437 (<http://data.cma.cn/en>). The 17 climatic factors could be classified into

438 temperature-related, wind-related, pressure-related, precipitation-related,
439 humidity-related and sunshine-related factors. (Table S21; Table S22).

440 PCAs of the climatic factors showed that PC1 (accounting for 53.2% of the total
441 variance) separated Liuzhou from Qinzhou, Nanning and Baise, while PC2
442 (accounting for 25.8% of the total variance) split Baise from Qinzhou, Nanning and
443 Liuzhou (Figure 7b). To examine the contributions of climatic factors to PC1 and PC2,
444 we loaded them in the PCA plot (Figure 7c). Temperature-related factors were the
445 main variables contributing to PC1, including mean minimum temperature (16.88%),
446 mean temperature (16.32%) and mean maximum temperature (14.50%), and
447 precipitation-related factors mainly contributed to PC2, including daily precipitation
448 (27.29%) and maximum daily precipitation (19.75%) (Figure 7d).

449 To examine the detailed differences in temperature- and precipitation-related
450 factors in these four locations, we plotted the monthly observations of mean minimum
451 temperature, mean temperature, mean maximum temperature, daily precipitation and
452 maximum daily precipitation (main contributors to PC1 and PC2) from 2018 to 2020
453 (Figure 7e, f; Figure S12; Table S22). The mean temperature of Liuzhou was much
454 lower than those of the other locations, especially in the two colder quarters of the
455 year. Additionally, daily precipitation was lower in Baise than in the other locations,
456 especially in early spring. All of these results suggested that relatively low
457 temperature and precipitation during the cold season imposes some degree of stress
458 on the plants and thus stimulated the production of the desired terpenoids in *C.*
459 *camphora*.

460



461
 462 **Figure 7** Analyses of climatic factors in different planting locations. (a) Geographical distribution of *C.*
 463 *camphora* planting locations, including Qinzhou, Nanning, Baise and Liuzhou. (b) Principal component
 464 analyses (PCA) of seventeen climatic factors in the four planting locations in 2018, 2019 and 2020. (c)
 465 The loadings of climatic factors in the PCA plot. The colours of the arrows represent the percentages of
 466 the contributions of climatic factors to the PCs. (d) Histograms of the percentages of the contributions of
 467 different climatic factors to PC1 and PC2. The red dashed lines indicate the average contributions of
 468 different climatic factors. Only the top eight climatic factors are shown. (e) Monthly observations of the
 469 mean temperature in the four planting locations. Single and double asterisks indicate statistically
 470 significance levels of $P < 0.05$ and $P < 0.01$, respectively, between Liuzhou and Qinzhou/Nanning
 471 (paired-sample Student's *t* test). (f) Monthly observations of daily precipitation in the four planting
 472 locations. A single asterisk indicates the statistically significance levels of $P < 0.05$ between Baise and
 473 Qinzhou/Nanning (paired-sample Student's *t* test).

474

475 Discussion

476 Here, by decoding the genome of the camphor tree, we revealed that magnoliids are a
 477 sister group to the clade of eudicots and monocots. The two rounds of WGD identified

478 in *C. camphora* were dated to ca. 85.66 Mya and 137.90 Mya, respectively. The
479 former was shared with Lauraceae species, and the latter occurred before the
480 divergence of Lauraceae and Calycanthaceae. We found that rapidly evolving TD
481 genes play key roles in the synthesis of secondary metabolites, especially for
482 monoterpenes and sesquiterpenes. By analysing volatile metabolites in leaves
483 sampled from plants of the same genotype grown in four different locations, we found
484 higher accumulation of the key volatile metabolites in regions with lower temperature
485 and precipitation in the cold season, which was attributed to the differential expression
486 of genes related to the MVA and MEP pathways as well as their downstream steps in
487 terpene biosynthesis. Our study confirmed that abiotic stress contributes to the
488 development of top-geoh herbs, laying a theoretical foundation for policy making on the
489 agroforestry applications of camphor trees.

490 In addition to releasing the first chromosome-level genome of this significant
491 economic tree species, our study is innovative in two regards. First, it is among the
492 very few innovative three-dimensional evaluations of the top-geoh herbalism of a TCM
493 species, integrating phytochemical, genetic and climatic analyses of camphor tree
494 germplasm (Li et al., 2017). Second, our study is the first to fix the genotypic variation
495 of the germplasm so that it is feasible to investigate how climatic factors alone affect
496 the accumulation of metabolites (Li et al., 2020; Mandim et al., 2021). By integrating
497 these two novel approaches, our study provides an example of how to
498 comprehensively scrutinize the genetic and climatic factors affecting the composition
499 of secondary metabolites.

500 The dominant climatic factors affecting the secondary metabolites of the camphor
501 tree are not always the key factors affecting in other traditional herbs. For example,
502 humidity and sunshine time are the chief limiting factors in the production of artemisinin
503 in *Artemisia annua* L. (Li et al., 2017). Additionally, lower temperature in the coldest
504 quarter imposes stress on camphor tree and increases the production of desired
505 volatile compounds. In other cases, a higher temperature imposes stress and
506 enhances the production of desired metabolites (Liu et al., 2020). The limiting
507 ecological and climatic factors depended on the native ranges of the herbs and climatic
508 conditions during their growing season (Körner, 2021). A thorough investigation of
509 each specific case would be beneficial for decision making.

510 Some caveats need to be considered when interpreting our results. First, broader
511 planting of the same genotype (i.e., covering all provinces in South China and even
512 some Southeast Asian countries) would provide a thorough understanding of the
513 optimal climatic variables resulting in the greatest consistency and efficacy of the
514 medicinal components of camphor tree (Sharma et al., 2020). Second, the further
515 experimental verification of the effect of temperature on metabolite contents and the
516 functional validation of selected candidate genes (such as *TPS-b*, *TPS-g*, or *TPS-a*) of
517 the biosynthetic pathway under controlled laboratory conditions would enhance our
518 conclusions (Lau and Sattely, 2015; Nett et al., 2020). Third, soil characteristics
519 (including nutritional status, humidity and rhizosphere microorganisms, etc.) are
520 crucial for the accumulation of secondary metabolites (Ciancio et al., 2019; de Vries et

521 al., 2020). However, owing to the absence of appropriate data for assessing these
522 characteristics, we overlooked ecological factors such as soil conditions. Further
523 studies addressing the abovementioned limitations would provide an in-depth
524 framework for understanding the genetic and environmental factors related to
525 top-geoherbalism.

526 Taken together, our results lay a theoretical foundation for the optimal production of
527 this economically significant tree species. The distributional range of camphor tree
528 largely overlaps with the land and maritime portions of the silk road of the Belt and
529 Road Initiative (Hinsley et al., 2020); thus, products obtained from camphor tree, such
530 as TCMs or essential oil, show a high chance of being exported to connected countries
531 in the Middle West, Western Europe and even North Africa. As tissue culture methods
532 for camphor trees are well established and the growth rate of the trees is relatively fast
533 (Shi et al., 2010), the commercial cultivation of trees *ex situ* is probably a sustainable
534 and economic method in addition to importation (Brinckmann, 2015). Thus, our
535 research will provide guidance for policy making, genotype selection and the
536 optimization of climatic conditions for growth by domestic and international
537 government stakeholders, farmers, merchandisers and consumers.

538

539 **Methods**

540 **Plant materials**

541 The sequences utilized for *de novo* genome assembly of the genome were obtained
542 from the fresh leaves of a single camphor tree (*C. camphora* var. *linaloolifera* Fujita;
543 NO.95), grown at Guangxi Forestry Research Institute.

544 Tissue-cultured seedlings were planted in four locations in Guangxi Province in
545 China in May 2018, including Qinzhou (21°58'52"N, 108°39'14"E), Nanning
546 (22°49'00"N, 108°19'39"E), Baise (23°54'09"N, 106°37'06"E) and Liuzhou
547 (24°19'35.0"N, 109°25'41"E). Fresh leaves were collected from the four locations for
548 RNA-Seq analyses and volatile compound quantification in November 2020.

549

550 **DNA sequencing**

551 High-molecular-weight (HMW) genomic DNA was extracted using a DNeasy Plant
552 Mini Kit (Qiagen, USA), and 50 µg of HMW genomic DNA was prepared to generate
553 SMRTbellTM libraries with a 20 kb insert size. Subsequently, PacBio circular
554 consensus sequencing (CCS) data were produced on the PacBio Sequel II platform.
555 Hi-C libraries were constructed from the tender leaves of *C. camphora* with fragments
556 labelled with biotin and sequenced on the Illumina NovaSeq 6000 platform.

557

558 **RNA sequencing**

559 Total RNA was extracted from each sample by using an RNAPrep Pure Plant kit
560 (TIANGEN, Beijing, China) according to the user manual. cDNA was synthesized from
561 20 µg of total RNA using Rever Tra Ace (TOYOBO, Osaka, Japan) with oligo (dT)
562 primers following the user manual. High-throughput sequencing was then performed
563 on the Illumina NovaSeq 6000 platform.

564

565 **De novo genome assembly and quality assessment**

566 The *C. camphora* genome was assembled by integrating the sequencing data
567 obtained with PacBio CCS technology and the Hi-C method using Hifiasm (Cheng et
568 al., 2021) with the default parameters. We assembled two contig-level genomes,
569 including a monoploid genome (haplotype A) and an allele-defined genome
570 (haplotype B). Before Hi-C scaffolding, we filtered the redundant contigs from the
571 contig-level genomes by using Purge_haplotigs (Roach et al., 2018). The Hi-C reads
572 were assessed with the HiC-Pro program (Servant et al., 2015) and uniquely mapped
573 to the contig assemblies. Juicer tools (Durand et al., 2016) and 3D-DNA pipelines
574 (Dudchenko et al., 2017) were used to perform chromosome scaffolding. The BUSCO
575 (Seppey et al., 2019) method was used to evaluate the completeness of the
576 chromosome-level genomes.

577

578 **Repetitive sequences and gene annotation**

579 We used the EDTA pipeline (Ou et al., 2019) to annotate transposable elements in the
580 *C. camphora* genome, including LTR, TIR and nonTIR elements. LAI assessment and
581 LTR insertion time estimation were performed by LTR_retriever (Ou and Jiang, 2018)
582 with the synonymous substitution rate set as 3.02e-9 (Cui et al., 2006). TRF software
583 (Benson, 1999) with modified parameters (“trf 1 1 2 80 5 200 2000”) was used to
584 identify tandem repeats.

585 For gene model annotation, we trained *ab initio* gene predictors, including
586 AUGUSTUS (Stanke and Morgenstern, 2005) and SNAP (Korf, 2004), on the
587 repeat-masked genome using a combination of protein and transcript data. We used
588 the annotated proteome data of *A. thaliana*, *L. chinense* (Chen et al., 2019), *C.*
589 *kanehirae* (Chaw et al., 2019) and *P. americana* (Rendón-Anaya et al., 2019) and the
590 Swiss-Prot database as the protein data. We employed RNA-Seq data from the four
591 locations as the transcript data. To train AUGUSTUS, BRAKER2 (Bruna et al., 2021)
592 was applied with the transcript data from aligned RNA-Seq bam files produced by
593 Hisat2 (Kim et al., 2015). SNAP was trained under MAKER (Cantarel et al., 2008) with
594 two iterations. Transcript data were supplied in the form of a *de novo* assembled
595 transcriptome generated in Trinity (Haas et al., 2013) and a reference-based
596 assembly generated by StringTie (Pertea et al., 2016). After training, the AUGUSTUS
597 and SNAP results were fed into MAKER again along with all other data to produced
598 synthesized gene models.

599 Functional annotations of the protein-coding sequences were obtained via BLASTP
600 (“-evalue 1e-10”) searches against entries in both the NR and Swiss-Prot databases.
601 The prediction of gene sequence motifs and structural domains was performed using
602 InterProScan (Jones et al., 2014). The annotations of the GO terms and KEGG
603 pathways of the genes were obtained from eggNOG-mapper (Huerta-Cepas et al.,
604 2017).

605

606 **Phylogenetic analyses and estimation of divergent times**

607 A total of 16 plant species, including five magnoliids (*C. camphora*, *C. kanehirae*, *P.*
608 *americana*, *Ch. salicifolius* and *L. chinense*), four monocots (*Zea mays*, *Oryza sativa*,

609 *Ananas comosus* and *Musa acuminata*), five eudicots (*A. thaliana*, *Populus*
610 *trichocarpa*, *Medicago truncatula*, *Solanum lycopersicum* and *V. vinifera*) and two
611 ANA-grade species (*Nymphaea colorata* and *Amborella trichopoda*) were used to
612 infer the phylogenetic tree. All genomes except for that of *Ch. salicifolius*
613 (http://xhhuanglab.cn/data/Chimonanthus_salicifolius.html) were downloaded from
614 JGI (<ftp://ftp.jgi-psf.org/pub/compngen/phytozome/v12.0/>) and Ensembl Plants
615 (<http://plants.ensembl.org/info/data/ftp/index.html>). Paralogues and orthologues were
616 identified among the 16 species by using the OrthoFinder pipeline (Emms and Kelly,
617 2019) with the default parameters, and the protein sequences of the 172 identified
618 single-copy orthologous genes were used for the construction of the phylogenetic tree.
619 The concatenated amino acid sequences were aligned with MAFFT (Kato and
620 Standley, 2013) and trimmed with trimAl (Capella-Gutiérrez et al., 2015). A maximum
621 likelihood (ML) phylogenetic tree was constructed using IQ-TREE (Nguyen et al.,
622 2015) with ultrafast bootstrapping (-bb 1000), using *N. colorata* and *A. trichopoda* as
623 outgroups. The best-fitting substitution models were selected by ModelFinder
624 (Kalyaanamoorthy et al., 2017). In addition, ASTRAL-III v5.7.3 (Zhang et al., 2018)
625 was applied to infer the coalescence-based species tree with 172 gene trees. The
626 species tree was then used as an input to estimate the divergence time in the
627 MCMCTree program in the PAML package (Yang et al., 2007). The calibration time
628 was obtained from TimeTree (Kumar et al., 2017): 107-135 Mya for the divergence of
629 *V. vinifera* and *A. thaliana*, 42-52 Mya for *Z. mays* and *O. sativa*, 97-116 Mya for *O.*
630 *sativa* and *M. acuminata* and 173-199 Mya for *A. trichopoda* and *A. thaliana*. The
631 expansion and contraction of gene families were inferred with CAFÉ (De Bie et al.,
632 2006) based on the chronogram of the 16 species

633

634 **Genome duplication and syntenic analyses**

635 To identify the pattern of genome-wide duplications in *C. camphora*, we divided
636 duplicated genes into five categories, WGD, TD, PD (duplicated genes separated by
637 less than 10 genes on the same chromosome), TRD, and DSD (the remaining
638 duplicates other than the four specified types) gene, using DupGen_Finder (Qiao et
639 al., 2019) with the default parameters. The *Ka*, *Ks*, and *Ka/Ks* values were estimated
640 for duplicated gene pairs based on the YN model in *KaKs_Calculator2* (Wang et al.,
641 2010), followed by the conversion of amino acid alignments into the corresponding
642 codon alignments with PAL2NAL (Suyama et al., 2006). The genes in the five
643 duplicate categories were further subjected to GO and KEGG analyses with the R
644 package clusterProfiler (Yu et al., 2012). The enriched items were selected according
645 to an FDR criterion of 0.05. The dating of ancient WGDs and orthologue divergence
646 were estimated based on the formula $T = Ks/2r$, where *Ks* refers to the synonymous
647 substitutions per site, and *r* (3.02e-9) is the synonymous substitution rate for
648 magnoliids (Cui et al., 2006).

649 Genomic synteny blocks to be employed for intra- and interspecies comparisons
650 among magnoliids were identified with MCscan software (Tang et al., 2008). We
651 performed all-against-all LAST analyses (Kielbasa et al., 2011) and chained the LAST
652 hits according to a distance cut-off of 10 genes, requiring at least five gene pairs per

653 synteny block. The syntenic “depth” function implemented in MCscan was applied to
654 estimate the duplication histories of the respective genomes. Genomic synteny was
655 visualized with the Python version of MCScan (Tang et al., 2008), the R package
656 Rldeogram (Hao et al., 2020) and Circos (Krzywinski et al., 2009).

657

658 **Gene expression profiling**

659 The raw RNA-Seq data were filtered by using FASTP (Chen et al., 2018). The clean
660 data were aligned to our assembled *C. camphora* genome with Hisat2 (Kim et al.,
661 2015), and the quantification of gene expression was calculated with StringTie (Pertea
662 et al., 2015). The Python script preDE.py built into StringTie was used to convert the
663 quantification results into a count matrix. DEGs were detected with the DESeq2 R
664 package (Love et al., 2014) with an FDR < 0.05.

665

666 **TPS gene family**

667 *TPS* genes are classified into seven subfamilies, including *TPS-a*, *TPS-b*, *TPS-c*,
668 *TPS-d*, *TPS-e*, *TPS-f* and *TPS-g* (Chen et al., 2011). The *TPS* genes included in the
669 *TPS-a* subfamily are responsible for forming 15-carbon sesquiterpenoids. The *TPS-b*
670 and *TPS-g* superfamilies encode the enzymes producing 10-carbon monoterpenoids.
671 The *TPS-c*, *TPS-e* and *TPS-f* subfamilies encode diterpene synthases, which
672 catalyse the formation of 20-carbon isoprenoids. The *TPS-d* subfamily is gymnosperm
673 specific and encodes enzymes involved in the production of 20-carbon isoprenoids
674 (Martin et al., 2004). The *TPS* genes were predicted based on both their conserved
675 domains (PF01397 and PF03936) and BLAST analyses. Conserved domains were
676 used as search queries against the predicted proteome using hmmsearch in HMMER
677 (<https://www.ebi.ac.uk/Tools/hmmer/>). *TPS* protein sequences from *A. thaliana* and *C.*
678 *kanehirae* were used as queries to identify the *TPS* genes of *C. camphora*, *P.*
679 *americana*, *L. chinense* and *V. vinifera*. The protein sequence hits of *TPS* genes were
680 aligned with MAFFT (Kato and Standley, 2013) and trimmed with trimAl
681 (Capella-Gutierrez et al., 2009). The *TPS* gene tree was constructed using RAxML
682 (Stamatakis, 2014) with 1,000 bootstrap replicates. The *TPS-c* subfamily was
683 designated as the outgroup. The distribution of *TPS* genes on the chromosomes was
684 visualized in TBtools (Chen et al., 2020).

685

686 **Identification of genes involved in the MVA and MEP pathways**

687 The MVA pathway involves six gene families, including the *acyl-coenzyme*
688 *A-cholesterol acyl-transferase (ACAT)*, *hydroxymethylglutaryl coenzyme A synthase*
689 *(HMGS)*, *hydroxymethylglutaryl coenzyme A reductase (HMGR)*, *mevalonate kinase*
690 *(MVK)*, *phospho-mevalonate kinase (PMK)*, and *mevalonate diphosphate*
691 *decarboxylase (MVD)* genes. Seven gene families are involved in the MEP pathway,
692 including the *1-deoxy-D-xylulose 5-phosphate synthase (DXS)*, *1-deoxy-D-xylulose*
693 *5-phosphate reductoisomerase (DXR)*, *2-C-methyl-D-erythritol-4-phosphate*
694 *cytidyltransferase (MCT)*, *4-(cytidine-5-diphospho)-2-C-methyl-D-erythritol kinase*
695 *(CMK)*, *MDS*, *(E)-4-hydroxy-3-methyl-but-2-enyl-pyrophosphate synthase (HDS)* and
696 *(E)-4-hydroxy-3-methyl-but-2-enyl-pyrophosphate reductase (HDR)* genes. The

697 genes in both the MVA and MEP pathways are well documented in the model plants.
698 To identify candidate genes related to the two pathways in the *C. camphora* genome,
699 we collected the protein sequences of genes in the MVA and MEP pathways identified
700 in *A. thaliana*. Using each *A. thaliana* gene as a query sequence, BLASTP (“-evaluate
701 1e-10”) analyses was performed to identify orthologous genes in *C. camphora*.

702

703 **Determination of volatile metabolites**

704 Six biological replicates were sampled in each location. The samples were ground
705 into powder in liquid nitrogen. Two grams of the powder was transferred to a 20 ml
706 headspace vial. The vials were sealed using crimp-top caps with TFE-silicone
707 headspace septa. In solid-phase microextraction (SPME) analyses, each vial was
708 placed at 60°C for 12 min, and a 65 µm
709 divinylbenzene/carboxene/polydimethylsiloxane fibre (Supelco, Bellefonte, PA, USA)
710 was then exposed to the headspace of the sample for 30 min at 60°C. Volatile
711 metabolites were detected by MetWare (<http://www.metware.cn/>) based on the Agilent
712 7890B-7000D platform. The desorption of the volatile metabolites from the fibre
713 coating was carried out in the injection port of the GC apparatus at 250°C for 10 min in
714 spitless mode. The identification and quantification of volatile metabolites were carried
715 out with a 30 m x 0.25 mm x 1.0 µm DB-5MS (5% phenyl-polymethylsiloxane)
716 capillary column. Helium was used as the carrier gas at a linear velocity of 1.0 ml/min.
717 The oven temperature was programmed to increase from 40°C (6 min) at 5°C/min
718 until it reached 280°C, where it was held for 5 min. Mass spectra were recorded in
719 electron impact (EI) ionization mode at 70 eV. The quadrupole mass detector, ion
720 source and transfer line temperatures were set at 150, 230 and 280°C, respectively.
721 Volatile compounds were identified by comparing the mass spectra with the data
722 system library (MWGC) and linear retention index.

723

724 **Climatic factor collection and analyses**

725 Data on 17 climatic factors from Qinzhou, Nanning, Baise and Liuzhou from 2018 to
726 2020 were downloaded from the National Meteorological Information Centre
727 (<http://data.cma.cn/en>). The analyses of the climatic factors were performed in the R
728 package FactoMineR (Lê et al., 2008).

729

730 **Funding information**

731 This study was supported by the National Key Research and Development Program
732 of China (Grant No. 2020YFA0907900), Genomic Studies on the Differences in the
733 Secondary Metabolism of Camphor Tree under Different Site conditions (Grant No.
734 JA-20-04-07 and Grant No. 202102), the National Natural Science Foundation of
735 China (Grant No. 32070242), the Shenzhen Science and Technology Program (Grant
736 No. KQTD2016113010482651), special funds for science technology innovation and
737 industrial development of Shenzhen Dapeng New District (Grant No. RC201901-05
738 and Grant No. PT201901-19), the China Postdoctoral Science Foundation (Grant No.
739 2020M672904), the Basic and Applied Basic Research Fund of Guangdong (Grant No.
740 2020A1515110912) and the USDA Agricultural Research Service Research

741 Participation Program of the Oak Ridge Institute for Science and Education (ORISE)
742 (Grant No. DE-AC05-06OR23100).

743

744 **Conflict of interest**

745 No conflict of interest was declared.

746

747 **Author contributions**

748 L.W., C.L. K.X.L. and R.H.J. conceived and designed the study; R.H.J., X.L.C., C.S.Z.,
749 P.W. and K.X.L. prepared the materials; C.L., X.L.C., X.Z.L., D.P. and X.X.H.
750 performed data analyses; R.H.J., X.L.C., D.E.H, C.L. and L.W. wrote the manuscript;
751 all authors read and approved the final draft.

752

753 **Data availability**

754 All the raw sequence reads of *C. camphora* have been deposited in NCBI under the
755 BioProject accession number PRJNA761572. The *C. camphora* genome assembly
756 and annotations have been deposited on the cyVerse platform
757 (https://data.cyverse.org/dav-anon/iplant/home/licheng_caas/C.camphora_genome).

758

759 **Reference**

- 760 Brinckmann, J.A. (2015) Geographical indications for medicinal plants: Globalization,
761 climate change, quality and market implications for geo-authentic botanicals.
762 *World J. Trad. Chinese Med.* **1**,16-23.
- 763 Benson, G. (1999) Tandem repeats finder: a program to analyze DNA sequences.
764 *Nucleic Acids Res.* **27**,573-580.
- 765 Bottoni, M., Milani, F., Mozzo, M., Radice Kolloffel, D.A., Papini, A., Fratini, F., Maggi,
766 F. and Santagostini, L. (2021) Sub-tissue localization of phytochemicals in
767 *Cinnamomum camphora* (L.) J. Presl. growing in Northern Italy. *Plants* **10**,1008.
- 768 Bruna, T., Hoff, K.J., Lomsadze, A., Stanke, M. and Borodovsky, M. (2021) BRAKER2:
769 automatic eukaryotic genome annotation with GeneMark-EP+ and AUGUSTUS
770 supported by a protein database. *NAR Genom. Bioinform.* **3**,a108.
- 771 Cantarel, B.L., Korf, I., Robb, S.M., Parra, G., Ross, E., Moore, B., Holt, C., Sanchez,
772 A.A. and Yandell, M. (2008) MAKER: an easy-to-use annotation pipeline
773 designed for emerging model organism genomes. *Genome Res.* **18**,188-196.
- 774 Capella-Gutiérrez, S., Silla-Martinez, J.M. and Gabaldón, T. (2009) TrimAl: a tool for
775 automated alignment trimming in large-scale phylogenetic analyses.
776 *Bioinformatics* **25**,1972-1973.
- 777 Chaw, S., Liu, Y., Wu, Y., Wang, H., Lin, C.I., Wu, C., Ke, H., Chang, L., Hsu, C.,
778 Yang, H., Sudianto, E., Hsu, M., Wu, K., Wang, L., Leebens-Mack, J.H. and Tsai,
779 I.J. (2019) Stout camphor tree genome fills gaps in understanding of flowering
780 plant genome evolution. *Nat. Plants* **5**,63-73.
- 781 Chen, C., Chen, H., Zhang, Y., Thomas, H.R., Frank, M.H., He, Y. and Xia, R. (2020)
782 TBtools: An Integrative Toolkit developed for interactive analyses of big biological
783 data. *Mol. Plant* **13**,1194-1202.
- 784 Chen, C., Zheng, Y., Liu, S., Zhong, Y., Wu, Y., Li, J., Xu, L. and Xu, M. (2017) The

- 785 complete chloroplast genome of *Cinnamomum camphora* and its comparison
786 with related Lauraceae species. *PeerJ* **5**,e3820.
- 787 Chen, C., Zhong, Y., Yu, F. (2020) Deep sequencing identifies miRNAs and their
788 target genes involved in the biosynthesis of terpenoids in *Cinnamomum*
789 *camphora*. *Ind. Crop Prod.* **145**,111853.
- 790 Chen, F., Tholl, D., Bohlmann, J. and Pichersky, E. (2011) The family of terpene
791 synthases in plants: a mid-size family of genes for specialized metabolism that is
792 highly diversified throughout the kingdom. *Plant J.* **66**,212-229.
- 793 Chen, J., Hao, Z., Guang, X., Zhao, C., Wang, P., Xue, L., Zhu, Q., Yang, L., Sheng,
794 Y., Zhou, Y., Xu, H., Xie, H., Long, X., Zhang, J., Wang, Z., Shi, M., Lu, Y., Liu, S.,
795 Guan, L., Zhu, Q., Yang, L., Ge, S., Cheng, T., Laux, T., Gao, Q., Peng, Y., Liu,
796 N., Yang, S. and Shi, J. (2019) *Liriodendron* genome sheds light on angiosperm
797 phylogeny and species-pair differentiation. *Nat. Plants* **5**,18-25.
- 798 Chen, S., Sun, W., Xiong, Y., Jiang, Y., Liu, X., Liao, X., Zhang, D., Jiang, S., Li, Y.,
799 Liu, B., Ma, L., Yu, X., He, L., Liu, B., Feng, J., Feng, L., Wang, Z., Zou, S., Lan,
800 S. and Liu, Z. (2020) The *Phoebe* genome sheds light on the evolution of
801 magnoliids. *Hortic. Res.* **7**,146.
- 802 Chen, S., Zhou, Y., Chen, Y. and Gu, J. (2018) Fastp: an ultra-fast all-in-one FASTQ
803 preprocessor. *Bioinformatics*, **34**, i884-i890.
- 804 Chen, Y., Li, Z., Zhao, Y., Gao, M., Wang, J., Liu, K., Wang, X., Wu, L., Jiao, Y., Xu, Z.,
805 He, W., Zhang, Q., Liang, C., Hsiao, Y., Zhang, D., Lan, S., Huang, L., Xu, W.,
806 Tsai, W., Liu, Z., Van de Peer, Y. and Wang, Y. (2020) The *Litsea* genome and
807 the evolution of the laurel family. *Nat. Commun.* **11**,1675.
- 808 Cheng, H., Concepcion, G.T., Feng, X., Zhang, H. and Li, H. (2021)
809 Haplotype-resolved *de novo* assembly using phased assembly graphs with
810 hifiasm. *Nat. Methods* **18**,170-175.
- 811 Ciancio, A., Pieterse, C.M.J. and Mercado-Blanco, J. Editorial: Harnessing useful
812 rhizosphere microorganisms for pathogen and pest biocontrol - second edition.
813 *Front. Microbiol.* **10**,1935.
- 814 Consultation Shenzhen Limu Information (2021) China's linalool industry market
815 development scale and forecast in 2021.
- 816 Cui, L., Wall, P.K., Leebens-Mack, J.H., Lindsay, B.G., Soltis, D.E., Doyle, J.J., Soltis,
817 P.S., Carlson, J.E., Arumuganathan, K., Barakat, A., Albert, V.A., Ma, H. and
818 DePamphilis, C.W. (2006) Widespread genome duplications throughout the
819 history of flowering plants. *Genome Res.* **16**,738-749.
- 820 De Bie, T., Cristianini, N., Demuth, J.P. and Hahn, M.W. (2006) CAFÉ: a
821 computational tool for the study of gene family evolution. *Bioinformatics* **22**,
822 1269-1271.
- 823 de Vries, F.T., Griffiths, R.I., Knight, C.G., Nicolitch, O. and Williams, A. (2020)
824 Harnessing rhizosphere microbiomes for drought-resilient crop production.
825 *Science* **368**,270-274.
- 826 Dudchenko, O., Batra, S.S., Omer, A.D., Nyquist, S.K., Hoeger, M., Durand, N.C.,
827 Shamim, M.S., Machol, I., Lander, E.S., Aiden, A.P. and Aiden, E.L. (2017) *De*
828 *nov* assembly of the *Aedes aegypti* genome using Hi-C yields

- 829 chromosome-length scaffolds. *Science* **356**,92-95.
- 830 Durand, N.C., Shamim, M.S., Machol, I., Rao, S.S., Huntley, M.H., Lander, E.S. and
831 Aiden, E.L. (2016) Juicer provides a one-click system for analyzing
832 loop-resolution Hi-C experiments. *Cell Syst.* **3**,95-98.
- 833 Eggersdorfer, M. (2000) *Terpenes*". *Ullmann's Encyclopedia of Industrial Chemistry*.
- 834 Emms, D.M. and Kelly, S. (2019) OrthoFinder: phylogenetic orthology inference for
835 comparative genomics. *Genome Biol.* **20**,238.
- 836 Endress, P.K. and Doyle, J.A. (2009) Reconstructing the ancestral angiosperm flower
837 and its initial specializations. *Am. J. Bot.* **96**,22-66.
- 838 Haas, B.J., Papanicolaou, A., Yassour, M., Grabherr, M., Blood, P.D., Bowden, J.,
839 Couger, M.B., Eccles, D., Li, B., Lieber, M., MacManes, M.D., Ott, M., Orvis, J.,
840 Pochet, N., Strozzi, F., Weeks, N., Westerman, R., William, T., Dewey, C.N.,
841 Henschel, R., LeDuc, R.D., Friedman, N. and Regev, A. (2013) *De novo*
842 transcript sequence reconstruction from RNA-seq using the Trinity platform for
843 reference generation and analyses. *Nat. Protoc.* **8**,1494-1512.
- 844 Hamidpour, R., Hamidpour, S., Hamidpour, M. and Shahlari, M. (2012) Camphor
845 (*Cinnamomum camphora*), a traditional remedy with the history of treating
846 several diseases. *Int. J. Case Rep. Images* **4**,86.
- 847 Hao, Z., Lv, D., Ge, Y., Shi, J., Weijers, D., Yu, G., Chen, J. (2020) Rldeogram:
848 drawing SVG graphics to visualize and map genome-wide data on the idiograms.
849 *PeerJ Comput. Sci.* **6**, e251.
- 850 Hinsley, A., Milner-Gulland, E.J., Cooney, R., Timoshyna, A., Ruan, X.D. and Lee, T.M.
851 (2020) Building sustainability into the Belt and Road Initiative's Traditional
852 Chinese Medicine trade. *Nat. Sustain.* **3**,96-100.
- 853 Hou, J., Zhang, J., Zhang, B., Jin, X., Zhang, H. and Jin, Z. (2020) Transcriptional
854 analyses of metabolic pathways and regulatory mechanisms of essential oil
855 biosynthesis in the leaves of *Cinnamomum camphora* (L.) Presl. *Front. Genet.*
856 **11**,598714.
- 857 Hu, L., Xu, Z., Wang, M., Fan, R., Yuan, D., Wu, B., Wu, H., Qin, X., Yan, L., Tan, L.,
858 Sim, S., Li, W., Saski, C.A., Daniell, H., Wendel, J.F., Lindsey, K., Zhang, X., Hao,
859 C. and Jin, S. (2019) The chromosome-scale reference genome of black pepper
860 provides insight into piperine biosynthesis. *Nat. Commun.* **10**,4702.
- 861 Huang, L. (2012) *Molecular Pharmacognosy*. Shanghai Scientific and Technical
862 Publishers.
- 863 Huerta-Cepas, J., Forslund, K., Coelho, L.P., Szklarczyk, D., Jensen, L.J., von Mering,
864 C. and Bork, P. (2017) Fast genome-wide functional annotation through orthology
865 assignment by eggNOG-Mapper. *Mol. Biol. Evol.* **34**,2115-2122.
- 866 Jones, P., Binns, D., Chang, H.Y., Fraser, M., Li, W., McAnulla, C., McWilliam, H.,
867 Maslen, J., Mitchell, A., Nuka, G., Pesseat, S., Quinn, A.F., Sangrador-Vegas, A.,
868 Scheremetjew, M., Yong, S.Y., Lopez, R. and Hunter, S. (2014) InterProScan 5:
869 genome-scale protein function classification. *Bioinformatics* **30**,1236-1240.
- 870 Kalyaanamoorthy, S., Minh, B.Q., Wong, T.K.F., von Haeseler, A. and Jermin, L.S.
871 (2017) ModelFinder: fast model selection for accurate phylogenetic estimates.
872 *Nat. Methods* **14**, 587-589.

- 873 Katoh, K. and Standley, D.M. (2013) MAFFT multiple sequence alignment software
874 version 7: improvements in performance and usability. *Mol. Biol. Evol.*
875 **30**,772-780.
- 876 Kielbasa, S.M., Wan, R., Sato, K., Horton, P. and Frith, M.C. (2011) Adaptive seeds
877 tame genomic sequence comparison. *Genome Res.* **21**, 487-493.
- 878 Kim, D., Langmead, B. and Salzberg, S.L. (2015) HISAT: a fast spliced aligner with
879 low memory requirements. *Nat. Methods* **12**,357-360.
- 880 Körner C. (2021) The cold range limit of trees. *Trends Ecol. Evol.* **13**,S0169-S5347.
- 881 Korf, I. (2004) Gene finding in novel genomes. *BMC Bioinformatics* **5**,59.
- 882 Krzywinski, M., Schein, J., Birol, I., Connors, J., Gascoyne, R., Horsman, D., Jones,
883 S.J. and Marra, M.A. (2009) Circos: an information aesthetic for comparative
884 genomics. *Genome Res.* **19**, 1639-1645.
- 885 Lau, W. and Sattely, E.S. (2015) Six enzymes from mayapple that complete the
886 biosynthetic pathway to the etoposide aglycone. *Science* **11**,1224-1228.
- 887 Lê S, Josse J and Husson F (2008) FactoMineR: An R package for multivariate
888 analyses. *J. Stat. Softw.* **25**,1-18.
- 889 Letizia, C.S., Cocchiara, J., Lalko, J. and Api, A.M. (2003) Fragrance material review
890 on linalool. *Food Chem. Toxicol.* **41**,943-964.
- 891 Li, C., He, Q., Zhang, F., Yu, J., Li, C., Zhao, T., Zhang, Y., Xie, Q., Su, B., Mei, L.,
892 Zhu, S, and Chen, J. (2019) Melatonin enhances cotton immunity to *Verticillium*
893 wilt via manipulating lignin and gossypol biosynthesis. *Plant J.* **100**,784-800.
- 894 Li, L., Josef, B.A., Liu, B., Zheng, S., Huang, L. and Chen, S. (2017)
895 Three-Dimensional Evaluation on Ecotypic Diversity of traditional Chinese
896 medicine: A case study of *Artemisia annua* L. *Front. Plant Sci.* **8**.
- 897 Li, Q., Ramasamy, S., Singh, P., Hagel, J.M., Dunemann, S.M., Chen, X., Chen, R.,
898 Yu, L., Tucker, J.E., Facchini, P.J. and Yeaman, S. (2020) Gene clustering and
899 copy number variation in alkaloid metabolic pathways of opium poppy. *Nat.*
900 *Commun.* **11**,1190.
- 901 Li, Y., Kong, D., Fu, Y., Sussman, M.R. and Wu, H. (2020) The effect of
902 developmental and environmental factors on secondary metabolites in medicinal
903 plants. *Plant Physiol. Biochem.* **148**,80-89.
- 904 Liu, L., Zuo, Z., Xu, F. and Wang, Y. (2020) Study on quality response to
905 environmental factors and geographical traceability of wild gentiana rigescens
906 Franch. *Front. Plant Sci.* **11**,1128.
- 907 Liu, X., Meng, Y., Zhang, Z., Wang, Y., Geng, X., Li, M., Li, Z. and Zhang, D. (2019)
908 Functional nano-catalyzed pyrolyzates from branch of *Cinnamomum camphora*.
909 *Saudi J. Biol. Sci.* **26**,1227-1246.
- 910 Love, M.I., Huber, W. and Anders, S. (2014) Moderated estimation of fold change and
911 dispersion for RNA-seq data with DESeq2. *Genome Biol.* **15**, 550.
- 912 Luo, Q., Xu, C., Zheng, T., Ma, Y., Li, Y. and Zuo, Z. (2021) Leaf morphological and
913 photosynthetic differences among four chemotypes of *Cinnamomum camphora*
914 in different seasons. *Ind. Crop Prod.* **169**,113651.
- 915 Lv, Q., Qiu, J., Liu, J., Li, Z., Zhang, W., Wang, Q., Fang, J., Pan, J., Chen, Z., Cheng,
916 W., Barker, M.S., Huang, X., Wei, X. and Cheng, K. (2020) The *Chimonanthus*

- 917 *salicifolius* genome provides insight into magnoliid evolution and flavonoid
918 biosynthesis. *Plant J.* **103**,1910-1923.
- 919 Mandim, F., Petropoulos, S.A., Dias, M.I., Pinela, J., Kostic, M., Soković, M.,
920 Santos-Buelga, C., Ferreira, I. and Barros, L. (2021) Seasonal variation in
921 bioactive properties and phenolic composition of cardoon (*Cynara cardunculus*
922 var. *altilis*) bracts. *Food Chem.* **336**,127744.
- 923 Massoni J, Couvreur TL and Sauquet H (2015) Five major shifts of diversification
924 through the long evolutionary history of Magnoliidae (angiosperms). *BMC Evol.*
925 *Biol.* **15**.
- 926 Moore, M.J., Bell, C.D., Soltis, P.S, and Soltis, D.E. (2007) Using plastid
927 genome-scale data to resolve enigmatic relationships among basal angiosperms.
928 *PNAS* **104**,19363-19368.
- 929 Nett, R.S., Lau, W. and Sattely, E.S. (2020) Discovery and engineering of colchicine
930 alkaloid biosynthesis. *Nature* **584**,48-153.
- 931 Nguyen, L.T., Schmidt, H.A., von Haeseler, A. and Minh, B.Q. (2015) IQ-TREE: a fast
932 and effective stochastic algorithm for estimating maximum-likelihood phylogenies.
933 *Mol. Biol. Evol.* **32**, 268-274.
- 934 Ou, S. and Jiang, N. (2018) LTR_retriever: A highly accurate and sensitive program
935 for identification of long terminal repeat retrotransposons. *Plant Physiol.*
936 **176**,1410-1422.
- 937 Ou, S., Su, W., Liao, Y., Chougule, K., Agda, J., Hellinga, A.J., Lugo, C., Elliott, T.A.,
938 Ware, D., Peterson, T., Jiang, N., Hirsch, C.N. and Hufford, M.B. (2019)
939 Benchmarking transposable element annotation methods for creation of a
940 streamlined, comprehensive pipeline. *Genome Biol.* **20**,275.
- 941 Palmer, J.D., Soltis, D.E. and Chase, M.W. (2004) The plant tree of life: an overview
942 and some points of view. *Am. J. Bot.* **91**,1437-1445.
- 943 Perteua, M., Kim, D., Perteua, G.M., Leek, J.T. and Salzberg, S.L. (2016)
944 Transcript-level expression analyses of RNA-seq experiments with HISAT,
945 StringTie and Ballgown. *Nat. Protoc.* **11**,1650-1667.
- 946 Qiao, X., Li, Q., Yin, H., Qi, K., Wang, R., Zhang S. and Paterson, A. (2019) Gene
947 duplication and evolution in recurring polyploidization-diploidization cycles in
948 plants. *Genome Biol.* **20**, 38.
- 949 Qin, L., Hu, Y., Wang, J., Wang, X., Zhao, R., Shan, H., Li, K., Xu, P., Wu, H., Yan, X.,
950 Liu, L., Yi, X., Wanke, S., Bowers, J.E., Leebens-Mack, J.H., DePamphilis, C.W.,
951 Soltis, P.S., Soltis, D.E., Kong, H. and Jiao, Y. (2021) Insights into angiosperm
952 evolution, floral development and chemical biosynthesis from the *Aristolochia*
953 *fimbriata* genome. *Nat. Plants* <https://doi.org/10.1038/s41477-021-00990-2>
- 954 Qiu, Y., Li, L., Wang, B., Xue, J., Hendry, T.A., Li, R., Brown, J.W., Liu, Y., Hudson,
955 G.T. and Chen, Z. (2010) Angiosperm phylogeny inferred from sequences of four
956 mitochondrial genes. *J. Syst. Evol.* **48**,391-425.
- 957 Ravindran, P.N., Nirmal Babu, K. and Shylaja, M. (2004) *Cinnamon and Cassia, the*
958 *Genus Cinnamomum*. USA:CRC Press: Boca Raton.
- 959 Rendón-Anaya, M., Ibarra-Laclette, E., Mendez-Bravo, A., Lan, T., Zheng, C.,
960 Carretero-Paulet, L., Perez-Torres, C.A., Chacon-Lopez, A., Hernandez-Guzman,

- 961 G., Chang, T.H., Farr, K.M., Barbazuk, W.B., Chamala, S., Mutwil, M., Shivhare,
962 D., Alvarez-Ponce, D., Mitter, N., Hayward, A., Fletcher, S., Rozas, J., Sanchez,
963 G.A., Kuhn, D., Barrientos-Priego, A.F., Salojarvi, J., Librado, P., Sankoff, D.,
964 Herrera-Estrella, A., Albert, V.A. and Herrera-Estrella, L. (2019) The avocado
965 genome informs deep angiosperm phylogeny, highlights introgressive
966 hybridization, and reveals pathogen-influenced gene space adaptation. *PNAS*
967 **116**,17081-17089.
- 968 Roach, M.J., Schmidt, S.A. and Borneman, A.R. (2018) Purge Haplotigs: allelic contig
969 reassignment for third-gen diploid genome assemblies. *BMC Bioinformatics*
970 **19**,460.
- 971 Seppey, M., Manni, M. and Zdobnov, E.M. (2019) BUSCO: Assessing Genome
972 Assembly and Annotation Completeness. *Methods Mol. Biol.* **1962**,227-245.
- 973 Servant, N., Varoquaux, N., Lajoie, B.R., Viara, E., Chen, C.J., Vert, J.P., Heard, E.,
974 Dekker, J. and Barillot, E. (2015) HiC-Pro: an optimized and flexible pipeline for
975 Hi-C data processing. *Genome Biol.* **16**,259.
- 976 Shang, J., Tian, J., Cheng, H., Yan, Q., Li, L., Jamal, A., Xu, Z., Xiang, L., Saski, C.A.,
977 Jin, S., Zhao, K., Liu, X. and Chen, L. (2020) The chromosome-level wintersweet
978 (*Chimonanthus praecox*) genome provides insights into floral scent biosynthesis
979 and flowering in winter. *Genome Biol.* **21**,200.
- 980 Sharma, S., Walia, S., Rathore, S., Kumar, P. and Kumar, R. (2020) Combined effect
981 of elevated CO₂ and temperature on growth, biomass and secondary metabolite
982 of *Hypericum perforatum* L. in a western Himalayan region. *J. Appl. Res. Med.*
983 *Aroma.* **16**,2214-7861.
- 984 Shi, X., Dai, X., Liu, G., Zhang, J., Ning, G. and Bao, M. (2010). Cyclic secondary
985 somatic embryogenesis and efficient plant regeneration in camphor tree
986 (*Cinnamomum camphora* L.). *In Vitro Cell Dev. Pl.* **46**,117-125.
- 987 Stamatakis, A. (2014) RAxML version 8: a tool for phylogenetic analyses and
988 post-analyses of large phylogenies. *Bioinformatics* **30**,1312-1313.
- 989 Stanke, M. and Morgenstern, B. (2005) AUGUSTUS: a web server for gene prediction
990 in eukaryotes that allows user-defined constraints. *Nucleic Acids Res.*
991 **33**,W465-W467.
- 992 Suyama, M., Torrents, D. and Bork, P. (2006) PAL2NAL: robust conversion of protein
993 sequence alignments into the corresponding codon alignments. *Nucleic Acids*
994 *Res.* **34**, W609-W612.
- 995 Tan, H., Hu, D., Song, J., Xu, Y., Cai, S., Chen, Q., Meng, Q., Li, S., Chen, S., Mao, Q.
996 and Xu, H. (2015) Distinguishing *Radix Angelica sinensis* from different regions
997 by HS-SFME/GC-MS. *Food Chem.* **186**,200-206.
- 998 Tang, H., Bowers, J.E., Wang, X., Ming, R., Alam, M. and Paterson, A.H. (2008)
999 Synteny and collinearity in plant genomes. *Science* **320**, 486-488.
- 1000 Tholl, D. (2015) Biosynthesis and biological functions of terpenoids in plants. *Adv*
1001 *Biochem. Eng. Biotechnol.* **148**,63-106.
- 1002 Tian, Z., Luo, Q. and Zuo, Z. (2021) Seasonal emission of monoterpenes from four
1003 chemotypes of *Cinnamomum camphora*. *Ind. Crop Prod.* **163**,113327.
- 1004 Wang, D., Zhang, Y., Zhang, Z., Zhu, J. and Yu, J. (2010) KaKs_Calculator 2.0: a

- 1005 toolkit incorporating gamma-series methods and sliding window strategies.
1006 *Genomics Proteom. Bioinform.* **8**, 77-80.
- 1007 Wu, Y., Xiao, F., Xu, H., Zhang, T. and Jiang, X. (2014) Genome Survey in
1008 *Cinnamomum camphora* L . Presl. *J. Plant. Genet. Resour.* **15**,149-152.
- 1009 Yang, Z. (2007) PAML 4, phylogenetic analyses by maximum likelihood. *Mol. Biol.*
1010 *Evol.* **24**,1586-1591.
- 1011 Yoshida, T., Muraki, S., Kawamura, H. and Komatsu, A. (1969) Minor constituents of
1012 Japanese ho-leaf oil the structures of (+)-tagetanol and (-)-trans-Hotrienol. *Agric.*
1013 *Biol. Chem.* **3**,343-352.
- 1014 Yu, G., Wang, L.G., Han, Y., and He, Q.Y. (2012) clusterProfiler: an R package for
1015 comparing biological themes among gene clusters. *OMICS* **16**, 284-287.
- 1016 Yuan, M., Yan, Z., Sun, D., Luo, X., Xie, L., Li, M., Wang, S., Shi, Q. and Zhang, Y.
1017 (2020) New insights into the impact of ecological factor on bioactivities and
1018 phytochemical composition of *Paeonia veitchii*. *Chem. Biodivers* **17**.
- 1019 Zeng, L., Zhang, Q., Sun, R., Kong, H., Zhang, N. and Ma, H. (2014) Resolution of
1020 deep angiosperm phylogeny using conserved nuclear genes and estimates of
1021 early divergence times. *Nat. Commun.* **5**,4956.
- 1022 Zhang, C., Rabiee, M., Sayyari, E. and Mirarab, S. (2018) ASTRAL-III: polynomial
1023 time species tree reconstruction from partially resolved gene trees. *BMC*
1024 *Bioinformatics* **19**,153.
- 1025 Zhang, Z., Wu, X., Lai, Y., Li, X., Zhang, D. and Chen, Y. (2020) Efficient extraction of
1026 bioenergy from *Cinnamomum camphora* leaves. *Front. Energy Res.* **8**.
- 1027 Zhao, Z., Guo, P. and Brand, E. (2012) The formation of daodi medicinal materials. *J.*
1028 *Ethnopharmacol.* **140**,476-481.
- 1029 Zhou, F. and Pichersky, E. (2020) More is better: the diversity of terpene metabolism
1030 in plants. *Curr. Opin. Plant Biol.* **55**,1-10.
1031
1032